COMMUNICATIONS IN APPLIED NUMERICAL METHODS, Vol. 8, 721–734 (1992)

A MULTIGRID METHOD FOR AN INVARIANT FORMULATION OF THE INCOMPRESSIBLE NAVIER–STOKES EQUATIONS IN GENERAL CO-ORDINATES

C. W. OOSTERLEE AND P. WESSELING
Delft University of Technology, P.O. Box 5031, 2600 GA Delft, The Netherlands

SUMMARY

The stationary incompressible Navier–Stokes equations are discretized with a finite volume method in curvilinear co-ordinates. The arbitrarily shaped domain is mapped onto a rectangular block, resulting in a boundary-fitted grid. In order to obtain accurate discretizations of the transformed equations, some requirements on geometric quantities should be met. The choice of velocity components is also of importance. Contravariant flux unknowns and pressure p are used as primary unknowns on a staggered grid arrangement.

The system of discretized equations is solved with a non-linear multigrid algorithm, into which a smoother, called Symmetric Coupled Gauss–Seidel, is implemented. Cell by cell, all unknowns in the grid cell are updated by solving four momentum equations and a continuity equation simultaneously. The solution algorithm shows satisfying average reduction factors for several domains.

1. INTRODUCTION

In order to compute flows in complex geometries, boundary-fitted co-ordinates may be used. In the development of numerical methods for the incompressible Navier–Stokes equations in general co-ordinates the following choices have to be made: (i) a staggered or non-staggered grid; (ii) velocity unknowns: Cartesian, contravariant or other; (iii) the interactive solution method.

On a non-staggered grid discretizations in general co-ordinates are less complicated than on a staggered grid. With non-staggered grids artificial stabilizing terms are required. Staggered grids easily lead to inherently stable and accurate discretizations. They have been used in general co-ordinates in References 1–3. If contravariant velocity unknowns are used, additional body force terms arise due to grid line curvature. In these terms the so-called Christoffel symbols occur. These involve the second derivative of the co-ordinate mapping, so that inaccuracies are to be feared on non-smooth grids. For this reason and because they are so many of them (18 in three dimensions) many authors avoid the Christoffel symbols by using Cartesian velocity components. This does not combine easily with staggered grids because these call for velocity components normal to co-ordinate lines, and this is usually done on non-staggered grids, which probably explains why this approach is more popular.

0748–8025/92/100721–14$12.00

Received August 1991
Revised January 1992

If a co-ordinate invariant discretization is formulated in Gibbs' vector notation, explicit occurrence of Christoffel symbols is avoided, as in Reference 2. Instead other geometric quantities appear implicitly, defining approximations to the Christoffel symbols.

The purpose of the present paper is twofold: firstly, to define a co-ordinate-invariant discretization on a staggered grid in standard tensor notation, showing that good accuracy can be obtained provided certain rules are followed; secondly, to present a multigrid method for the efficient solution of the resulting system of non-linear algebraic equations.

2. DISCRETIZATION IN GENERAL CURVILINEAR CO-ORDINATES

The transformation

$$\mathbf{x} = \mathbf{x}(\xi), \mathbf{x} \in \Omega, \xi \in G \tag{1}$$

maps a computational rectangular block G onto the physical domain Ω; $\mathbf{x}$, ξ are Cartesian and boundary-conforming curvilinear co-ordinates, respectively. Covariant base vectors $\mathbf{a}_{(\alpha)}$, contravariant base vectors $\mathbf{a}^{(\alpha)}$, the covariant and contravariant metric tensors $g_{\alpha\beta}$ and $g^{\alpha\beta}$ are defined as

$$\mathbf{a}_{(\alpha)} = \frac{\partial \mathbf{x}}{\partial \xi^\alpha}, \qquad \mathbf{a}^{(\alpha)} = \frac{\partial \xi^\alpha}{\partial \mathbf{x}}, \qquad g_{\alpha\beta} = \mathbf{a}_{(\alpha)} \cdot \mathbf{a}_{(\beta)}, \qquad g^{\alpha\beta} = \mathbf{a}^{(\alpha)} \cdot \mathbf{a}^{(\beta)} \tag{2}$$

The determinant of the covariant metric tensor $g_{\alpha\beta}$ is denoted by g; $\sqrt{g}$ equals the Jacobian of the transformation, given by

$$J = \sqrt{g} = \mathbf{a}_{(1)} \cdot (\mathbf{a}_{(2)} \wedge \mathbf{a}_{(3)}) \tag{3}$$

Tensor notation proves indispensable for formulating physical conservation laws in general co-ordinates. An introduction to tensor analysis can be found in References 4–6, for example. For completeness we summarize some basic tools used.

For the covariant derivative of a contravariant tensor of rank one and for the covariant derivative of a contravariant tensor of rank two it can be shown that:

$$Q^\alpha_{,\beta} = \frac{\partial Q^\alpha}{\partial \xi^\beta} + \left\{ \begin{matrix} \alpha \\ \gamma\beta \end{matrix} \right\} Q^\gamma; \qquad Q^{\alpha\beta}_{,\beta} = \frac{1}{\sqrt{g}} \frac{\partial \sqrt{g} Q^{\alpha\beta}}{\partial \xi^\beta} + \left\{ \begin{matrix} \alpha \\ \gamma\beta \end{matrix} \right\} Q^{\gamma\beta} \tag{4}$$

where $\{^\alpha_{\gamma\beta}\}$ represents the Christoffel symbol of the second kind, defined by

$$\left\{ \begin{matrix} \alpha \\ \gamma\beta \end{matrix} \right\} = \mathbf{a}^{(\alpha)} \cdot \frac{\partial \mathbf{a}_{(\gamma)}}{\partial \xi^\beta} = \frac{\partial \xi^\alpha}{\partial x^\delta} \frac{\partial^2 x^\delta}{\partial \xi^\gamma \partial \xi^\beta} \tag{5}$$

Application of the divergence theorem to a constant vector field gives

$$\int_\Omega Q^\alpha_{,\alpha} \, d\Omega = \oint_S Q^\alpha \, dS_\alpha = q^\beta \oint_S a^{(\alpha)}_\beta \, dS_\alpha = 0 \tag{6}$$

where $d\Omega$ is the infinitesimal volume element given by

$$d\Omega = \sqrt{g} \, d\xi^1 \, d\xi^2 \ldots d\xi^d \tag{7}$$

d being the number of spatial dimensions, and dS_α represents the (physical) surface element. Since $q^\beta = constant$ is arbitrary, this leads to the following geometric identity:

$$\oint_S a^{(\alpha)}_\beta \, dS_\alpha = 0 \tag{8}$$

The governing equations are the incompressible Navier–Stokes equations. Using contravariant velocity components, the co-ordinate-invariant formulation of the governing equations becomes

$$U^{\alpha}_{,\alpha} = 0 \tag{9}$$

and

$$T^{\alpha\beta}_{,\beta} \equiv (\rho U^{\alpha} U^{\beta})_{,\beta} + (g^{\alpha\beta} p)_{,\beta} - \tau^{\alpha\beta}_{,\beta} = \rho F^{\alpha} \tag{10}$$

where ρ is the fluid density and $\tau^{\alpha\beta}$ represents the deviatoric stress tensor given by

$$\tau^{\alpha\beta} = \mu(g^{\alpha\gamma} U^{\beta}_{,\gamma} + g^{\gamma\beta} U^{\alpha}_{,\gamma}) \tag{11}$$

with μ the viscosity coefficient.

We now turn to the discretization of (9) to (11) in two dimensions. We found that for accuracy reasons the following requirements should be met:

(i) The geometric identity (8) should be satisfied exactly for all cells.
(ii) When representing a constant velocity field $\mathbf{u}$ on the staggered grid in terms of its contravariant components U^{α}, and recomputing $\mathbf{u}$ from U^{α}, the original vector field $\mathbf{u}$ should be recovered exactly.
(iii) Uniform flow fields should satisfy the discrete equations exactly.

The first two requirements can be met if one proceeds as follows. The base vectors $\mathbf{a}_{(\alpha)}$ are computed according to

$$a^{\beta}_{(1)} = \frac{\delta x^{\beta}}{\delta \xi^{1}}, \qquad a^{\beta}_{(2)} = \frac{\delta x^{\beta}}{\delta \xi^{2}} \tag{12}$$

in the U^2- and U^1-points, respectively, in the staggered grid. Furthermore,

$$\sqrt{g} = a^{1}_{(1)} a^{2}_{(2)} - a^{2}_{(1)} a^{1}_{(2)}, \qquad \mathbf{a}^{(1)} = \frac{1}{\sqrt{g}} (a^{2}_{(2)}, -a^{1}_{(2)}), \qquad \mathbf{a}^{(2)} = \frac{1}{\sqrt{g}} (-a^{2}_{(1)}, a^{1}_{(1)}) \tag{13}$$

taking averages where required.

Integration of the incompressibility constraint over a pressure cell with centre at (0, 0) gives

$$\int_{\Omega} U^{\alpha}_{,\alpha} \, \mathrm{d}\Omega = \oint_{S} U^{\alpha} \, \mathrm{d}S_{\alpha} \tag{14}$$

Discretization of (14) gives

$$\oint_{S} U^{\alpha} \, \mathrm{d}S_{\alpha} \cong V^{1} \Big|_{-1,0}^{1,0} \delta\xi^{2} + V^{2} \Big|_{0,-1}^{0,1} \delta\xi^{1} \tag{15}$$

where $V^{\alpha} = \sqrt{g} U^{\alpha}$. Let $\mathbf{u}$ be a constant vector field. Substituting $V^{\alpha} = \sqrt{g} a^{(\alpha)}_{\beta} u^{\beta}$ and using (12) one finds that

$$V^{1} \Big|_{-1,0}^{1,0} \delta\xi^{2} + V^{2} \Big|_{0,-1}^{0,1} \delta\xi^{1} = 0 \tag{16}$$

so that requirement (i) is satisfied. Requirement (ii) is verified as follows. Let $\mathbf{w}^{\alpha}$ be a constant vector field. Its representation in terms of V^{α} on the staggered grid is $V^{\alpha} = \sqrt{g} a^{(\alpha)}_{\beta} w^{\beta}$. Hence, using (13),

$$V^{1} = a^{2}_{(2)} w^{1} - a^{1}_{(2)} w^{2}, \qquad V^{2} = -a^{2}_{(1)} w^{1} + a^{1}_{(1)} w^{2} \tag{17}$$

Now recompute the Cartesian components u^α from (17) in the cell vertices:

$$u^\alpha|_{1,1} = \frac{1}{2\sqrt{g}}|_{1,1}\{\Sigma_1(a^\alpha_{(1)}V^1) + \Sigma_2(a^\alpha_{(2)}V^2)\} \tag{18}$$

where Σ_1 indicates summation over grid points (1, 0) and (1, 2), and Σ_2 indicates summation over (0, 1) and (2, 1). Substitution of (17) in (18), and evaluation of $\sqrt{g}$ according to (13) results in

$$u^\alpha|_{1,1} = w^\alpha|_{1,1} \tag{19}$$

We also have (19) in cell centres (0, 0). Hence, requirement (ii) is satisfied. If U^α is used as primary unknown instead of V^α, (19) would not hold exactly, which is why the use of V^α is to be preferred. This is confirmed by numerical experiments on the Navier–Stokes equations. As a preparation for the discretization of the momentum equations we discuss the discretization of a general conservation law of the form

$$T^{\alpha\beta}_{,\beta} = f^\alpha \tag{20}$$

This equation is to be integrated over finite volumes. On the staggered grid used here, integration takes place over cells with vertices in U^2-points and centre in a U^1-point for $\alpha = 1$, and vice versa for $\alpha = 2$. Taking a cell with centre at (1, 0) as an example, using equation (4) and partial integration gives

$$\begin{aligned}\int_\Omega T^{1\beta}_{,\beta}\,\mathrm{d}\Omega &= \int_\Omega \frac{\partial\sqrt{g}T^{1\beta}}{\partial\xi^\beta}\,\mathrm{d}\xi^1\,\mathrm{d}\xi^2 + \int_\Omega \begin{Bmatrix}1\\ \gamma\beta\end{Bmatrix} T^{\gamma\beta}\sqrt{g}\,\mathrm{d}\xi^1\,\mathrm{d}\xi^2 \\ &\cong (\sqrt{g}T^{11}|\,{}^{\frac{2}{0}};{}^{0}_{0}\,\delta\xi^2 + (\sqrt{g}T^{12})|\,{}^{\frac{1}{1}};{}^{1}_{-1}\,\delta\xi^1 \\ &\quad + \left(\sqrt{g}\begin{Bmatrix}1\\ \gamma\beta\end{Bmatrix} T^{\gamma\beta}|_{1,0}\right)\delta\xi^1\,\delta\xi^2\end{aligned} \tag{21}$$

With $T^{\alpha\beta}_{,\beta}$ from (10) this is the discretization used for the momentum equations. It is found that the variable $V^\alpha = \sqrt{g}U_\alpha$ appears naturally in many places in (21).

In order to obtain equations suitable for multigrid solution some form of upwind discretization has to be used for the convection terms. In Cartesian co-ordinate systems the so-called hybrid scheme[7] is popular. For the convection terms a central difference scheme (CDS) is used if the mesh Reynolds number is smaller than 2, and a first-order upwind scheme (UDS) if it exceeds 2. For further discussion of the hybrid scheme, see Reference 8. In general co-ordinates it is not at all trivial how a hybrid scheme should be formulated and how the mesh Reynolds number should be defined, because of the occurrence of source terms and mixed derivatives in the viscous stress term. The criterion for switching between CDS and UDS will be generalized to general co-ordinates by requiring that the sum of coefficients arising from the viscous terms and the flux part (i.e. the part not involving Christoffel symbols) of the convection terms multiplying V^α in neighbouring points should be non-positive. This implies that a suitable definition of the mesh Reynolds number $\mathrm{Re}^{(i,j)}$ is that it is the ratio of the absolute magnitudes of the viscous term and the flux part of the convective term, discretized with a central scheme in point (i, j). If $\mathrm{Re}^{(i,j)} > 1$, UDS is used; if $\mathrm{Re}^{(i,j)} < 1$, CDS is used. Unlike the original hybrid scheme the contribution of the viscous stress tensor will be kept for all mesh Reynolds numbers. The volume integral remaining in the convective terms in general co-ordinates is discretized with a central scheme.

Convergence problems for the multigrid method are avoided by using a 'smooth' switch from central to upwind discretization:

$$\text{CONV.TERM} = (1 - \alpha^{(i,j)})\ \text{CENTRAL} + \alpha^{(i,j)}\ \text{UPWIND} \tag{22}$$

where $\alpha^{(i,j)} = \alpha(\text{Re}^{(i,j)})$ may be defined by

$$\begin{aligned} \text{Re}^{(i,j)} &< 0{\cdot}9 \ ;\alpha^{(i,j)} = 0 \\ 0{\cdot}9 \leqslant \text{Re}^{(i,j)} &\leqslant 1{\cdot}1 \ ;\alpha^{(i,j)} = 5\ \text{Re}^{(i,j)} - 4{\cdot}5 \\ \text{Re}^{(i,j)} &> 1{\cdot}1 \ ;\alpha^{(i,j)} = 1 \end{aligned} \tag{23}$$

The total number of variables linked together in a momentum equation is 19.

On a non-smooth grid, discretizing all Christoffel symbols according to (5) was found to cause a non-physical pressure distribution. This is avoided by eliminating the Christoffel symbols from the pressure term in (10) and (21) with the relation

$$\sqrt{g}\begin{Bmatrix} \alpha \\ \beta\gamma \end{Bmatrix} g^{\beta\gamma} = -\frac{\partial(\sqrt{g}g^{\alpha\beta})}{\partial \xi^{\beta}} \tag{24}$$

Figure 1 gives an example of a Poiseuille flow on an irregular grid.

The grid shown in (a), (b) gives the pressure distribution, where the Christoffel symbols in the pressure term are kept and discretized according to (5). The pressure distribution is not correct. Figure 1(c) shows the correct distribution obtained by using (24).

It remains to verify requirement (iii). Imposing boundary conditions such that the exact solution is a uniform flow in an arbitrary direction on the grids of Figure 9 and solving the discrete equations numerically results in the correct solution, showing empirically that (iii) is satisfied. However, when the mapping is non-differentiable, this is not the case. This can perhaps be remedied, but we will not pursue this further here. The sensitivity of the accuracy to details of the implementation of the geometric quantities in the case of non-differentiable

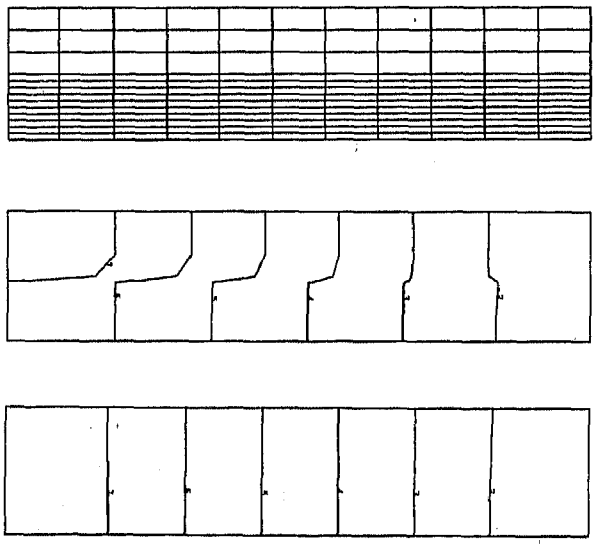

Figure 1. A Poiseuille flow, Re = 100: (a) the 11 × 13-grid; (b) the non-physical pressure using (5); (c) the physical pressure using (24)

co-ordinate mappings is illustrated by the following example. Straightforward approximation of the viscous stress leads to terms like

$$\tau^{11} = 2\mu(g^{11}U_{,1}^{1} + g^{12}U_{,2}^{1}) \tag{25}$$

$$\tau^{12} = \mu(g^{11}U_{,1}^{2} + g^{22}U_{,2}^{1}) \tag{26}$$

$$\tau^{22} = 2\mu(g^{12}U_{,1}^{2} + g^{22}U_{,2}^{2}) \tag{27}$$

By using the following identity:

$$-\frac{\partial g^{11}}{\partial \xi^1} = \begin{Bmatrix} 1 \\ 1\delta \end{Bmatrix} g^{\delta 1} + \begin{Bmatrix} 1 \\ 1\delta \end{Bmatrix} g^{1\delta} = 2\left(\begin{Bmatrix} 1 \\ 11 \end{Bmatrix} g^{11} + \begin{Bmatrix} 1 \\ 12 \end{Bmatrix} g^{21} \right) \tag{28}$$

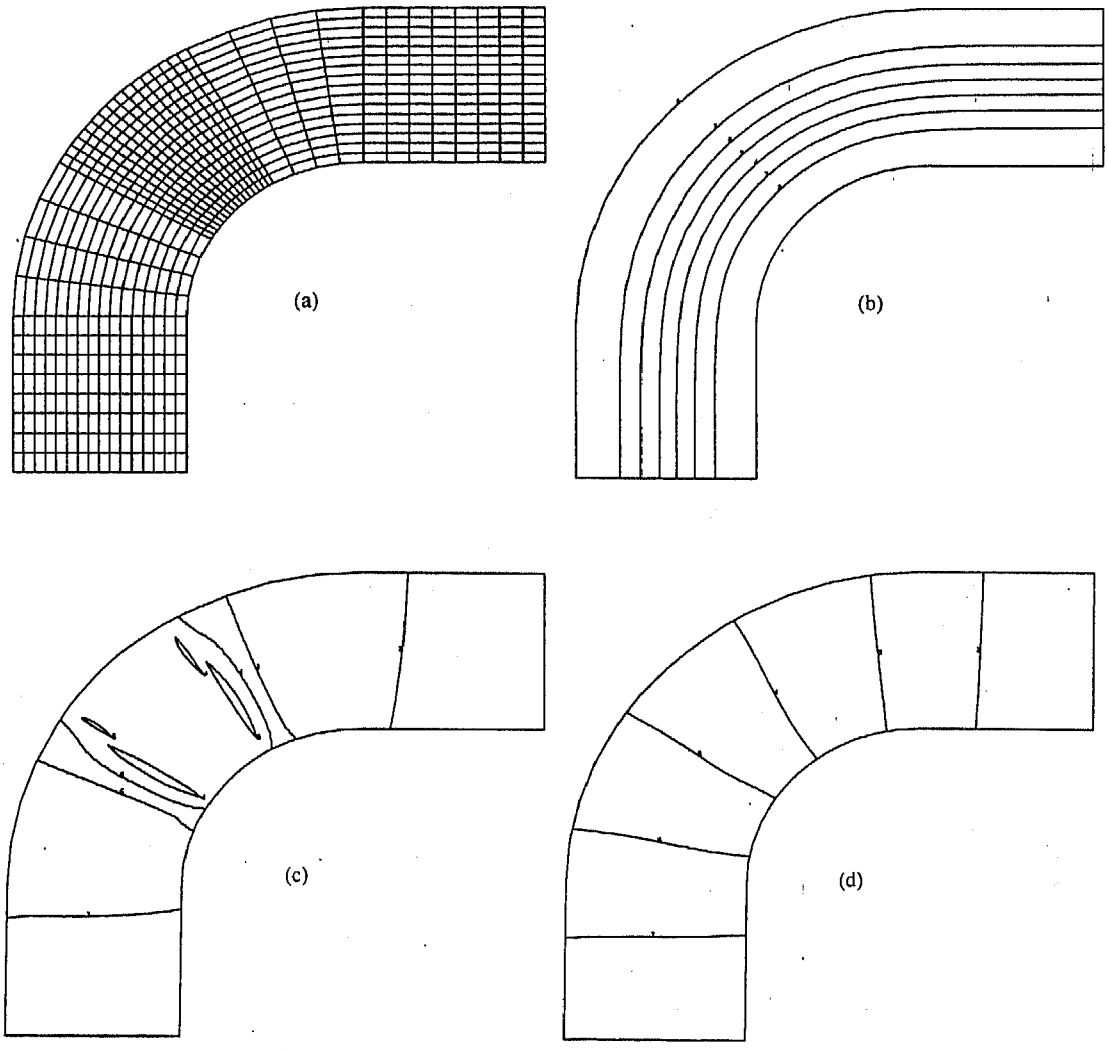

Figure 2. Flow through a bend-shaped channel: (a) the non-smooth (16 × 40) grid; (b) streamlines; (c) the non-physical pressure distribution discretizing (25)–(27); (d) the pressure distribution discretizing (26), (29) and (30)

τ^{11} and τ^{22} can be rewritten as

$$\tau^{11} + 2\mu * \left[(g^{11})^{3/2} \frac{\partial}{\partial \xi^1} \left(\frac{V^1}{\sqrt{g_{22}}} \right) + g^{12} \frac{\partial}{\partial \xi^2} \left(\frac{V^1}{\sqrt{g}} \right) + \frac{V^2}{\sqrt{g}} \left(g^{11} \begin{Bmatrix} 1 \\ 12 \end{Bmatrix} + g^{12} \begin{Bmatrix} 1 \\ 22 \end{Bmatrix} \right) \right] \tag{29}$$

$$\tau^{22} = 2\mu * \left[(g^{22})^{3/2} \frac{\partial}{\partial \xi^2} \left(\frac{V^2}{\sqrt{g_{11}}} \right) + g^{12} \frac{\partial}{\partial \xi^1} \left(\frac{V^2}{\sqrt{g}} \right) + \frac{V^1}{\sqrt{g}} \left(g^{12} \begin{Bmatrix} 2 \\ 11 \end{Bmatrix} + g^{22} \begin{Bmatrix} 2 \\ 21 \end{Bmatrix} \right) \right] \tag{30}$$

Both versions are applied to a test problem, a flow through a bend, where the physical domain is a non-smooth grid. Figure 2 shows that the second option is more accurate, so this version is used in the sequel.

3. THE MULTIGRID ALGORITHM

The standard non-linear multigrid algorithm is used in the form presented in Reference 9. A non-recursive well structured version (requiring only one GOTO statement in Fortran) is presented in References 10 and 11. Iteration should start with nested iteration for best efficiency, but this has not yet been implemented.

The smoothing method used here is the symmetric coupled Gauss–Seidel method (SCGS) with underrelaxation introduced in Reference 12. The variables are updated collectively cell by cell. Five discretized equations are solved simultaneously for an interior cell. Corrections are calculated and added to a current solution.

Prolongation and restriction operators are more or less dictated by the staggered grid arrangement. Prolongation operators are derived for all variables using bilinear interpolation.

The restricted coarse grid fluxes V^α are defined to be the mean of their two neighbouring fine grid fluxes. Coarse grid pressures are defined to be the mean of the four neighbouring fine grid pressures. In evaluating the coarse grid right-hand-side area weighting is used for the fine grid residuals, as follows:

$$r_{i,j}^{(1)k-1} = 1/8(r_{2i-2,2j}^{(1)k} + r_{2i-2,2j-1}^{(1)k} + r_{2i,2j}^{(1)k} + r_{2i,2j-1}^{(1)k}) + \tag{31}$$

$$1/4(r_{2i-1,2j}^{(1)k} + r_{2i-1,2j-1}^{(1)k}) \tag{32}$$

$$r_{i,j}^{(2)k-1} = 1/8(r_{2i,2j-2}^{(2)k} + r_{2i-1,2j-2}^{(2)k} + r_{2i,2j}^{(2)k} + r_{2i-1,2j}^{(2)k}) + \tag{33}$$

$$1/4(r_{2i,2j-1}^{(2)k} + r_{2i-1,2j-1}^{(2)k}) \tag{34}$$

$$r_{i,j}^{(3)k-1} = 1/4(r_{2i-1,2j}^{(3)k} + r_{2i-1,2j-1}^{(3)k} + r_{2i,2j}^{(3)k} + r_{2i,2j-1}^{(1)k}) \tag{35}$$

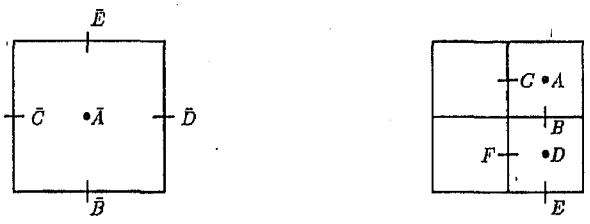

Figure 3. Definition of grid point numbering. The coarse grid cell shown is the union of the four fine grid cells shown. The grids are divided into triads with gridpoint indices:

$$\bar{A} = \bar{B} = \bar{C} = (i, j),\ \bar{D} = (i+1, j),\ \bar{E} = (i, j+1)$$

and

$$A = B = C = (2i, 2j),\ D = E = F = (2i, 2j-1)$$

The grid point numbering is given in Figure 3. The coarse grid is constructed by removing the even cell vertices from the next finer grid, and the geometric quantities are calculated as was done on the finest grid. Therefore requirement (i) derived in Section 2 is satisfied also on a coarse grid.

4. TEST PROBLEMS AND SOME RESULTS

The first test problem investigated is the driven cavity flow. Average reduction factors r are compared, defined as

$$r = \left(\frac{\| \text{res} \|_{20}}{\| \text{res} \|_0} \right)^{1/20} \tag{36}$$

i.e. the l_2-norm of the residual after 20 iterations divided by the l_2-norm of the starting residual. For the driven cavity flow, r is computed for a skewed cavity (i.e. a parallelogram) and a unit rectangular cavity, for several Reynolds numbers (Re). The starting vector is the zero solution on the finest grid. The number of presmoothing iterations *npre* is 1, the number of postsmoothing iterations *npost* is 1, the number of coarse grid relaxation iterations *ncrs* is 10. The results given are reduction factors for the W-cycle, which showed the best reduction factors, followed by the F and V cycle. As in Reference 13 different underrelaxation parameters α_k in the SCGS smoother are needed for different Reynolds numbers. For high Re we need to choose α_k different from Reference 13, probably because the stress term is not neglected in our hybrid scheme. For low Re (Re < 400) the SCGS smoother is lexicographical (i.e. sweeping along horizontal lines); for high Re the lexicographical sweep is followed by a sweep along vertical lines as in Reference 13. Tables I–IV give the reduction factors. In Tables III and IV an unusual improvement of the average reduction factors is observed when the grid is refined. This improvement is due to the fact that a hybrid scheme is used for the convective

Table I. Driven cavity (Re = 1), lexicographical SCGS, npre = npost = 1, W-cycle

Re = 1 $\alpha_k = 0{\cdot}7$	Levels	Grid	r, skewed	r, square
	4	16 × 16	0·331	0·288
	5	32 × 32	0·349	0·268
	6	64 × 64	0·360	0·316

Table II. Driven cavity (Re = 100), lexicographical SCGS, npre = npost = 1, W-cycle

Re = 100 $\alpha_k = 0{\cdot}7$	Levels	Grid	r, skewed	r, square
	4	16 × 16	0·390	0·328
	5	32 × 32	0·353	0·315
	6	64 × 64	0·345	0·310
	7	128 × 128	0·338	0·313

Table III. Driven cavity (Re = 400), alternating SCGS, npre = npost = 1, W-cycle

Re = 400 $\alpha_k = 0{\cdot}4$	Levels	Grid	r, skewed	r, square
	4	16 × 16	0·502	0·454
	5	32 × 32	0·445	0·446
	6	64 × 64	0·463	0·398
	7	128 × 128	0·310	0·310

Table IV. Driven cavity (Re = 1000), alternating SCGS, npre = npost = 1, W-cycle

Re = 1000 $\alpha_k = 0{\cdot}3$	Levels	Grid	r, skewed	r, square
	4	16 × 16	0·508	0·516
	5	32 × 32	0·619	0·565
	6	64 × 64	0·646	0·564
	7	128 × 128	0·710	0·517

terms, so the central difference scheme will be applied in large parts of the domain when the grid is very fine. This improves the convergence rate. Figures 4–7 show the streamlines and the pressure contours for the skewed cavity (skew angle 63°), obtained on the 64 × 64 grid. It looks as if r is bounded well away from 1 independent of the number of levels, except for Re = 1000; this effect is not there when the cavity is closer to a square. With a skew angle of 79°, $r = 0{\cdot}526$ on a 128 × 128 grid. The following test problems show the potentialities of the discretization method at the present stage of development. A flow at low Reynolds number through a straight pipe (equidistant grid, square cells), an L-shaped pipe and a nozzle flow are considered. Parabolic velocity profiles are prescribed at in- and outflow. This is unphysical of

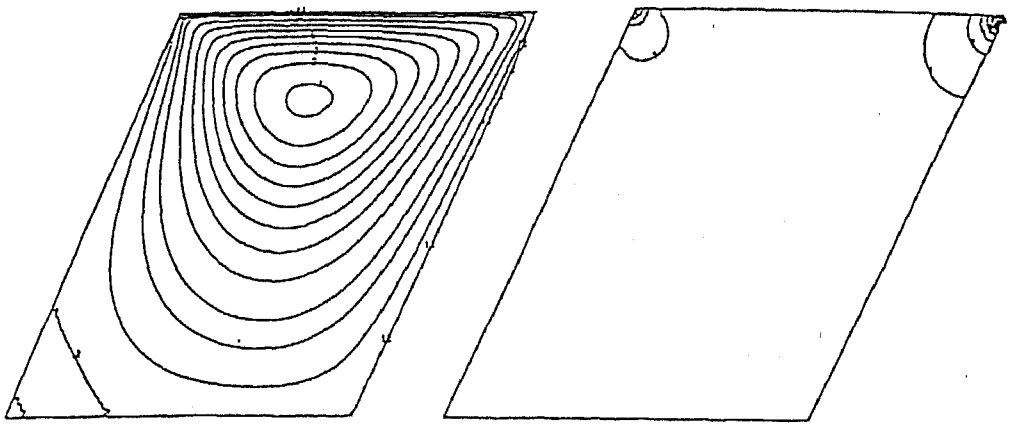

Figure 4. Streamlines and pressure contours for the skewed (under 63 degrees) driven cavity, Re = 1,64 × 64 grid

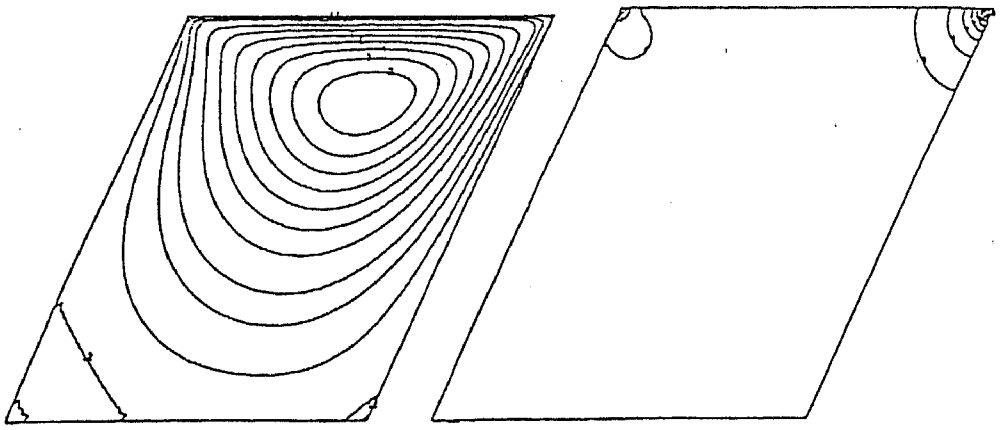

Figure 5. Streamlines and pressure contours for the skewed driven cavity, Re = 100, 64 × 64 grid

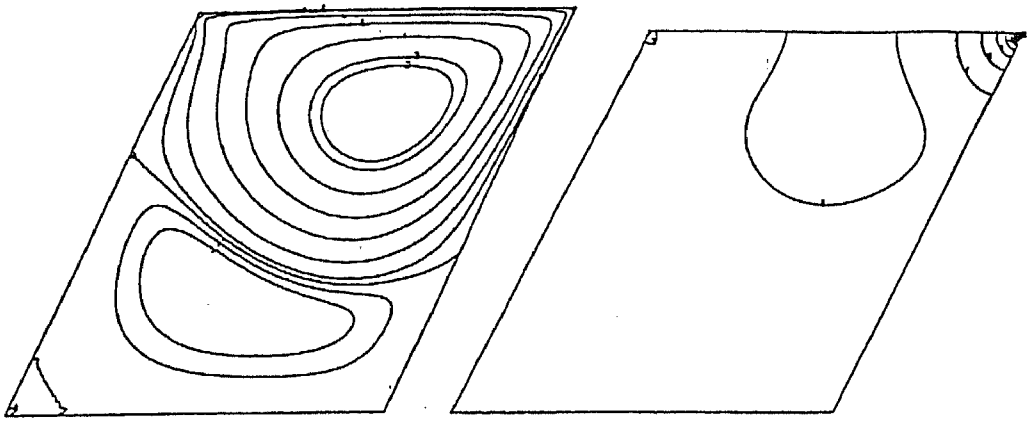

Figure 6. Streamlines and pressure contours for the skewed driven cavity, Re = 400, 64 × 64 grid

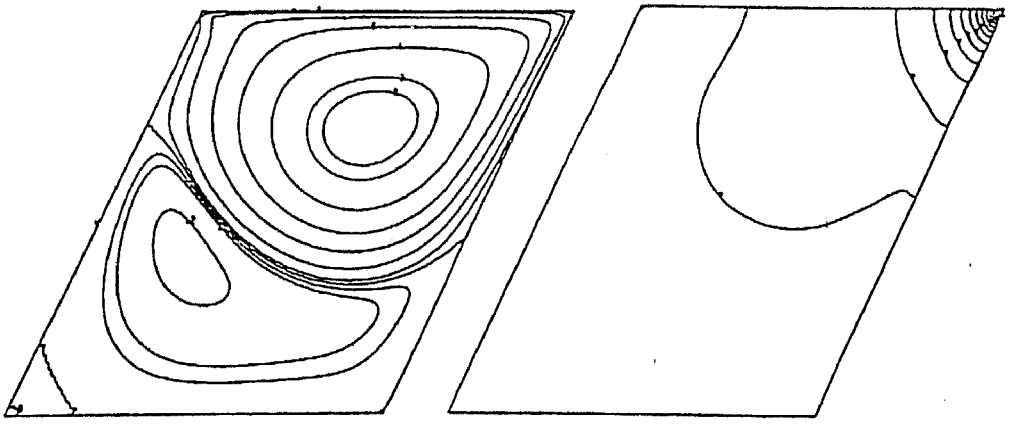

Figure 7. Streamlines and pressure contours for the skewed driven cavity, Re = 1000, 64 × 64 grid

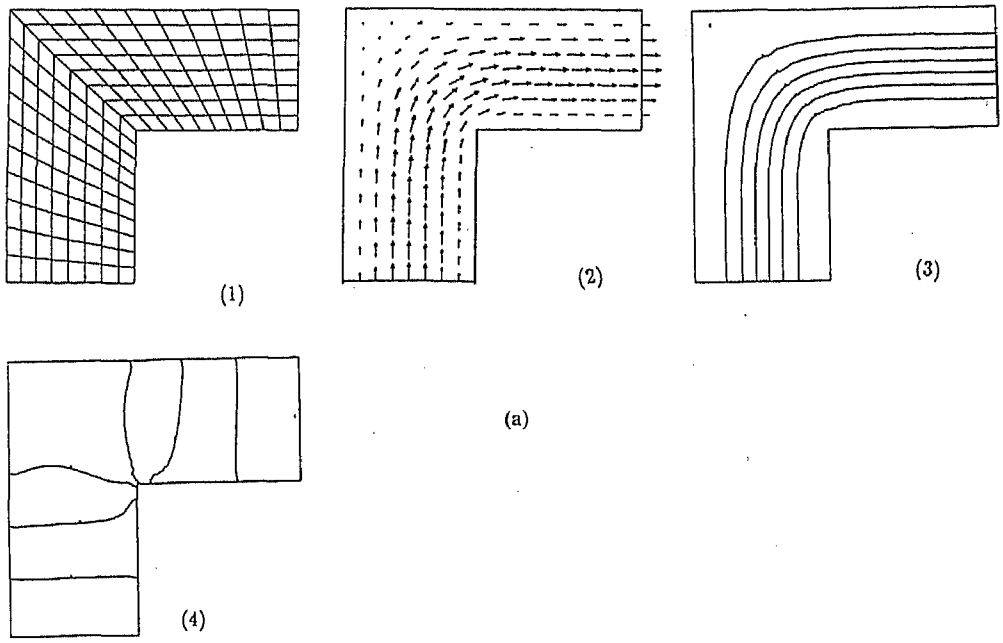

Figure 8(a). Flow through an L-shaped pipe: (1) the 8×20 grid, (2) flow pattern, (3) streamlines, (4) pressure

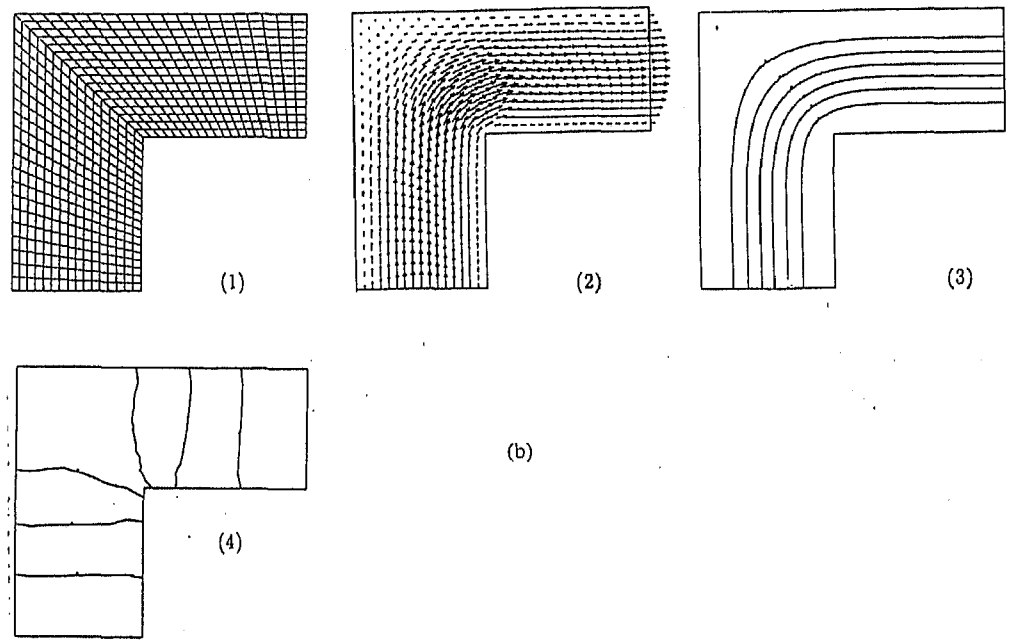

Figure 8(b). Flow through an L-shaped pipe: (1) the 16×40 grid, (2) flow pattern, (3) streamlines, (4) pressure

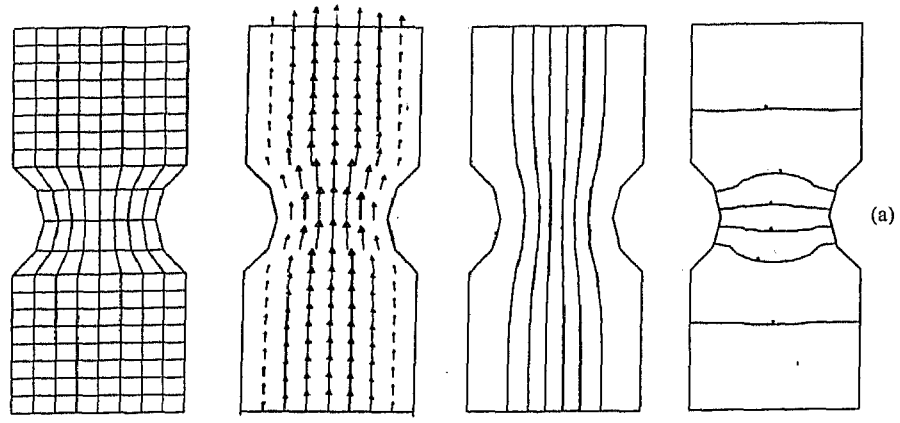

Figure 9(a). Flow through a nozzle: (1) the 8×20 grid, (2) flow pattern, (3) streamlines, (4) pressure

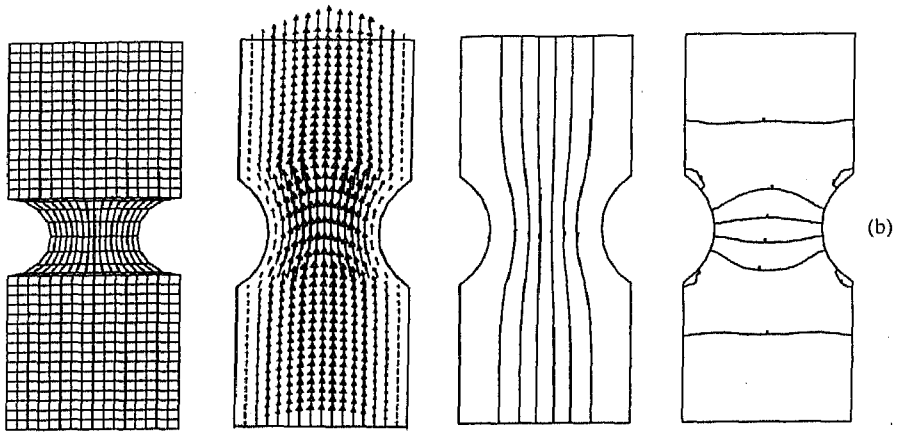

Figure 9(b). Flow through a nozzle: (1) the 16×40 grid, (2) flow pattern, (3) streamlines, (4) pressure

Table V. Channel flows at Re = 1, lexicographical SCGS, npre = npost = 1, W-cycle

Levels	Grid	r (pipe)	r (L-shape)	r (nozzle)
1 = sg	4×10	0·835	0·848	0·843
2	4×10	0·254	0·376	0·329
3	8×20	0·281	0·385	0·376
4	16×40	0·301	0·437	0·468

course, but of no concern here. Average reduction factors r are compared for these geometries for several grids. Table V shows the reduction factors for the W-cycle. The reduction factors for the other cycles did not differ much. The details for the MG-algorithm are: npre = 1, npost = 1, ncrs = 10, $s_k = 1$, Re = 1, lexicographical SCGS, $\alpha_k = 0{\cdot}7$. Figures 8 and 9 show grids, flow patterns, streamlines and pressure contours for the L-shape and nozzle geometry. It seems that for the nozzle reduction factors are not level-independent, but Figure 9 shows that the 16×40 grid is much more non-uniform than the 8×20 grid, which may be of greater consequence for r than the number of levels.

5. CONCLUSIONS

An invariant formulation of the incompressible Navier–Stokes equations has been presented in which Christoffel symbols occur. The discretization of the invariant formulation shows good results for many geometries and fairly non-uniform grids. A standard multigrid solution method is found to work well. A level-independent convergence rate has been found for the test problems. Reduction factors for rectangular and some more complex geometries do not seem to differ much.

The code is robust, especially for low Reynolds number flows. Then it is insensitive to large variations of the relaxation parameters. The convergence rate slows down with larger relaxation parameters for higher Reynolds numbers ($\geqslant 400$).

Further development of the code will include nested iteration and a line smoother to cope with stretched cells.

REFERENCES

1. L. Davidson and P. Hedberg, 'Mathematical derivation of a finite volume formulation for laminar flow in complex geometries', *Int. j. numer. methods fluids*, **9** 531–540 (1989).
2. M. Rosenfeld, D. Kwak and M. Vinokur, 'A solution method for the unsteady and incompressible Navier-Stokes equations in generalized coordinate systems', AIAA Paper 88-0718, 1988.
3. I. Demirdzic, A. D. Gosman, R. I. Issa and M. Peric, 'A calculation procedure for turbulent flow in complex geometries', *Comput. Fluids*, **15**(3) 251–273 (1987).
4. R. Aris, *Vectors, Tensors and the Basic Equations of Fluid Mechanics*, Prentice-Hall, Inc., Englewood Cliffs, N.J., 1962.
5. I. S. Sokolnikoff, *Tensor Analysis*, Wiley, 1964.
6. L. I. Sedov, *A Course in Continuum Mechanics*, Vol. I, 'Basic equations and analytical techniques', Wolters-Noordhoff Publishing, Groningen, The Netherlands, 1964.
7. D. B. Spalding, 'A novel finite difference formulation for differential expressions involving both first and second derivatives', *Int. j. numer. methods eng.*, **4**, 551–559 (1972).
8. S. V. Patankar, *Numerical Heat Transfer and Fluid Flow*, Hemisphere, Washington, 1980.
9. W. Hackbusch, *Multi-Grid Methods and Applications*, Springer, Berlin Heidelberg, 1985.
10. P. Wesseling, 'Two remarks on multigrid methods', in W. Hackbusch (Ed.), *Robust Multigrid Methods, Proceedings of the 4th GAMM-Seminar*, Kiel, 1988, pp. 209–216, *Notes on Numerical Fluid Mechanics*, **23**, Vieweg, Braunschweig, 1989.
11. P. Wesseling, 'Multigrid methods in computational fluid dynamics', *Z. Angew. Math. Mech.*, **70**, 337–348 (1990).
12. S. P. Vanka, 'Block-implicit multigrid solution of Navier-Stokes equations in primitive variables', *J. Comput. Phys.*, **65**, 138–158 (1986).
13. J. S. Rollett, D. F. Mayers and T. M. Shah, 'Analysis and application of an efficient line solver based upon the symmetrical coupled Gauss-Seidel scheme', Report Oxford Univ. Comput. Lab., 88/10, 1988.

14. Ch. Arakawa, A. O. Demuren, W. Rodi and B. Schönung, 'Application of multigrid, methods for the coupled and decoupled solution of the incompressible Navier-Stokes equations', in M. Deville (Ed.), *Proc. 7th GAMM Conf. on Num. Methods in Fluid Mech.*, Louvain-la-Neuve, Sept. 1987; *Notes on Numerical Fluid Mechanics,* **20**, 1988, Vieweg, Braunschweig, pp. 1–8.
15. A. Brandt, 'Guide to multigrid development', in W. Hackbusch and U. Trottenberg (Eds), *Multigrid Methods*, **960**, Springer Verlag, Berlin, 1982, pp. 220–312.
16. W. Rodi, S. Majundar and B. Schönung, 'Finite volume methods for two-dimensional incompressible flows with complex boundaries', *Comput. Methods Appl. Mech. Eng.*, **75**, 369–392 (1989).